AIP | The Journal of Chemical Physics

Absolute cross sections for dissociative electron attachment and dissociative ionization of cobalt tricarbonyl nitrosyl in the energy range from 0 eV to 140 eV

Sarah Engmann, Michal Stano, Peter Papp, Michael J. Brunger, Štefan Matejčík et al.

Citation: J. Chem. Phys. **138**, 044305 (2013); doi: 10.1063/1.4776756
View online: http://dx.doi.org/10.1063/1.4776756
View Table of Contents: http://jcp.aip.org/resource/1/JCPSA6/v138/i4
Published by the American Institute of Physics.

Absolute cross sections for dissociative electron attachment and dissociative ionization of cobalt tricarbonyl nitrosyl in the energy range from 0 eV to 140 eV

Sarah Engmann,[1] Michal Stano,[2] Peter Papp,[2] Michael J. Brunger,[3,4] Štefan Matejčík,[2,a)] and Oddur Ingólfsson[1,a)]

[1]*Science Institute and University of Iceland, Dunhagi 3, 107 Reykjavík, Iceland*
[2]*Department of Experimental Physics, Faculty of Mathematics, Physics and Informatics, Comenius University, Mlynska dolina F2, 84248 Bratislava, Slovakia*
[3]*ARC Centre for Antimatter-Matter Studies, CaPS, Flinders University, GPO Box 2100, Adelaide, SA 5001, Australia*
[4]*Institute of Mathematical Sciences, University of Malaya, Kuala Lumpur 5063, Malaysia*

(Received 5 October 2012; accepted 3 January 2013; published online 24 January 2013)

We report absolute dissociative electron attachment (DEA) and dissociative ionization (DI) cross sections for electron scattering from the focused electron beam induced deposition (FEBID) precursor $Co(CO)_3NO$ in the incident electron energy range from 0 to 140 eV. We find that DEA leads mainly to single carbonyl loss with a maximum cross section of 4.1×10^{-16} cm^2, while fragmentation through DI results mainly in the formation of the bare metal cation Co^+ with a maximum cross section close to 4.6×10^{-16} cm^2 at 70 eV. Though DEA proceeds in a narrow incident electron energy range, this energy range is found to overlap significantly with the expected energy distribution of secondary electrons (SEs) produced in FEBID. The DI process, on the other hand, is operative over a much wider energy range, but the overlap with the expected SE energy distribution, though significant, is found to be mainly in the threshold region of the individual DI processes. © *2013 American Institute of Physics*. [http://dx.doi.org/10.1063/1.4776756]

I. INTRODUCTION

Metallic cobalt is ferromagnetic and thus is useful in applications that exploit its magnetic properties, e.g., as a permanent magnet material. Its alloys are known to be corrosion and wear resistant and exhibit high strength even at elevated temperatures. Its metal complexes, particularly the carbonyl derivatives cobalt octacarbonyl and cobalt tricarbonyl nitrosyl, have proven to be useful for both homogeneous[1] and heterogeneous catalyses.[2] The high volatility of $Co_2(CO)_8$ and $Co(CO)_3NO$ make them suitable candidates for chemical vapour deposition (CVD), allowing the deposition of pure[3] or composite cobalt films for microelectronics and information technology.[4–6] With the advancement of nanotechnology tools and in particular focused electron beam induced deposition (FEBID) (for recent reviews on the method, see Utke *et al.*[7] and van Dorp and Hagen[8]), it has become possible to deposit more localized, three-dimensional structures. Cobalt octacarbonyl and cobalt tricarbonyl nitrosyl have thus been used in FEBID to deposit catalysts for carbon nanotube growth,[9] and to fabricate magnetic force microscopy (MFM) tips,[10,11] crossbar Hall nanosensors,[12] electrode contacts,[10] and cobalt nanowires.[13] While deposit purities of up to 95% have been demonstrated for $Co_2(CO)_8$,[14] there are currently several drawbacks limiting the use of this purely carbonyl containing cobalt precursor in FEBID. For instance, cobalt octacarbonyl exhibits poor stability under vacuum and it has a fairly low decomposition temperature (60 °C–70 °C).[15] In addition, spontaneous polymerization reactions may occur, changing the stochiometry of the precursor prior to deposition and causing a build up of pressure within the precursor reservoir.[13] Furthermore, commercially available cobalt carbonyl generally contains hexane as a stabilizing agent, increasing the unwanted hydrocarbon background pressure in the vacuum system. Recent research has thus focused on $Co(CO)_3NO$ as an alternative candidate for electron beam induced Co deposition,[13,16] as it combines high vapour pressure (100 Torr at 25 °C) with a relatively high decomposition temperature (130 °C–140 °C).

Most precursor molecules employed for FEBID have originally been designed for use in CVD,[7] where high deposit purity with respect to the metal content is reached at elevated temperatures through thermally induced metal-ligand bond rupture. In FEBID, however, although in some cases local beam induced heating may play a role,[17,18] the dissociation mechanism of the precursor molecules should be very different, i.e., be electron induced. In principle, the molecules should only be dissociated at the impact site of the electron beam, leaving behind a chemically and structurally well-defined deposit while the volatile ligand fragments are pumped away.

Unfortunately, although FEBID has proven to be a highly versatile nanofabrication technique, it still suffers from two major drawbacks, i.e., a broadening of the deposited structures relative to the primary electron (PE) beam and a low metal content of the deposited structures.[19] The low metal

a)Authors to whom correspondence should be addressed. Electronic addresses: stefan.matejcik@fmph.uniba.sk and odduring@hi.is.

content of the deposits may be traced back to one or more of the following; incomplete decomposition of the precursor molecules, co-deposition of the ligands, and contamination from residual gases. Broadening of the structures, on the other hand, is generally attributed to a flux of back-scattered electrons (BSE) and low energy secondary electrons (SE, E < 50 eV as per the usual definition) outside the focus point of the primary beam. These electrons are generated through elastic and inelastic scattering of the PE beam, from the deposit and the substrate, and are thus unavoidable in FEBID. Typically, the SE energy distribution, generated by high-energy electrons impinging on a substrate, peaks well below 10 eV. Note that the yield can be as high as 0.1 SE/PE/eV.[7,20] At those energies, dissociative electron attachment (DEA) is the only efficient fragmentation mechanism and, in that context, its potential role in FEBID has been discussed in some detail.[21–25] Although DEA is the only effective electron induced dissociation mechanism below the ionization limit of the respective molecules, SEs and BSEs, with incident energies close to and above the ionization limit of the respective molecules, can also cause fragmentation through dissociative ionization (DI). This is a non-resonant process, but can nonetheless be very efficient at fairly low incident energies (typically, in the range 10–50 eV).

It is still an open question as to which electrons and mechanisms are responsible for the dissociation in FEBID[7,8,26,27] with Monte Carlo (MC) simulations being increasingly used to model and elucidate the FEBID process (see, for example, Smith *et al.*[28]). The strength of this approach is that all primary electron trajectories, and subsequently generated SEs, can be traced together with their respective energies. The lack of relevant experimental cross sections, however, currently limit the reliability of those calculations, which generally incorporate simple generic cross section[7,29] models. Hence, at this time cross sections of, e.g., hydrocarbons are adapted to replace the unknown cross sections of the metal containing precursor molecules and, to our knowledge, DEA has never been explicitly included in the simulations, despite the high number of SEs that are known to be present with energies below 10 eV. Furthermore, the results of these simulations strongly depend on the shape of the input cross sections,[30] and thus even processes that are restricted to a narrow energy range may influence the outcome of the simulations significantly.

In this contribution, we present absolute DEA and DI cross sections for all available dissociation pathways upon electron impact on the FEBID precursor molecule $Co(CO)_3NO$, in the energy range from 0–140 eV.

II. EXPERIMENTAL DETAILS

A. Instrumental setup

The current experiments were performed with the crossed electron/molecular beam apparatus at the Comenius University, Bratislava,[31] under single collision conditions at room temperature. The molecular beam was generated by gas effusion through a stainless steel capillary and its pressure was monitored with an absolute capacitance pressure gauge (MKS Baratron, 0–7 Pa). The electron beam was generated with a trochoidal electron monochromator (FWHM 140 meV).[32] The electron energy scale was calibrated with respect to the 0 eV resonance of SF_6^-/SF_6 for negative ion detection, and the formation of Ar^+/Ar at 15.759 eV[33] for positive ion detection, prior to each measurement. Fragment ions were selected by a quadrupole mass analyser and detected in single counting mode. Cobalt tricarbonyl nitrosyl was purchased from Strem Chemicals, Bischheim, France and was used as received.

B. Accuracy of the estimated cross sections

Absolute cross sections for positive ion formation were calibrated relative to the cross section for Ar^+ given by Rejoub and co-workers with a stated accuracy of ±5%,[34] and absolute cross sections for the negative ion formation were calibrated relative to the cross section of SF_5^- from SF_6 at 300 K.[35] Explicit error margins are not given for the SF_5^- cross section,[35] but judging from error bars shown and their discussion these should be accurate within ±10%.

In the current experiment, the molecular beam is formed with a temperature regulated effusive molecular beam source (EMBS), i.e., a reservoir chamber connected to the collision chamber through a capillary. The pressure within the EMBS is regulated via a leak valve, and monitored with a Baratron. Using this setup, very stable pressure, with deviations of ≤3%, was achieved even over prolonged scans. The temperature of the chamber was monitored with a thermocouple and was constant at 302 K throughout the measurements.

The onset of the electron beam in the present experiment is primarily defined by its energy resolution, and in the energy range from about 0.2 to 10 eV the intensity is constant within ±7%. The cross section for the SF_5^- formation from SF_6 has its maximum at about 0.55 eV,[35] hence falls within this range. Thus, above 0.2 eV, intensity changes in the electron beam should not influence the DEA cross section values significantly. Close to 0 eV, however, the electron current can be up to 50% lower than measured at the plateau above 0.2 eV, potentially causing under estimation of the cross section for $[Co(CO)_2NO]^-$ at very low electron energies. In the higher energy range, relevant for the determination of the positive ion formation, the current drops gradually by about 10%, (from about 50 to 140 eV), but current fluctuations are found to be <±3% in this energy range. This does, however, not influence the estimate of the cross sections, as the measured Ar^+ ion yield is scaled to the absolute cross sections reported by Rejoub *et al.*[34] throughout the energy range prior to the calibration of the positive ion cross sections in the same energy range.

In the current experiment, the ion extraction field is kept below 1 V/cm to minimize its effect on the electron beam. This, can in turn cause reduced extraction efficiency for fragment ions that are formed with high kinetic energy release (KER) with respect to the thermal Ar^+ and SF_5^- [36] ions used for calibration. Direct information on the KER in electron induced dissociation of $Co(CO)_3NO$ is not available in the literature, however, Fieber-Erdmann *et al.*[37] have studied the

dissociation dynamics of positive ion formation from iron pentacarbonyl through photo-ionization in the energy range between 9.5–25 eV. In this study, they found the KER to vary between slightly above thermal to about 100 meV depending on the photon energy and the fragment formed. The authors concluded that the remaining energy must be distributed mainly into rotational and vibrational excitations of the fragments. While no KER data are available for $Co(CO)_3NO$, Sztaray and Baer[38] have modeled the internal energy distribution of the fragment ions after dissociation. Similar to what was deduced by Fieber-Erdmann *et al.*[37] for $Fe(CO)_5$, the fragment ions contain a considerable amount of internal energy after dissociation. Based on this and the fact that the bonding and dissociation mechanisms in $Co(CO)_3NO$ and $Fe(CO)_5$ are similar, we adopt the values reported by Fieber-Erdmann *et al.*[37] as a reasonable estimate of the KER in DI of the cobalt complex under study. In order to estimate the potential effect of the KER on the draw-out efficiency, we have simulated the extraction efficiency for individual fragments with different KER using the commercial program SIMION (8.0) and the actual geometry and extraction fields of our collision/extraction region. In the energy range from 50 to 100 meV, we find the extraction efficiency to be reduced by about 30%–60% relative to the respective thermal ions.

In DEA to $Co(CO)_3NO$, the total excess energy at the peak position of the ion yield for the individual fragments does generally not exceed 1 eV. Exceptions are the $CoCO^-$ and the Co^- formation through the higher lying resonance that peaks around 6 eV in the respective ion yields.[21] In these contributions, the KER might thus be higher. Due to the high mass of the negative ions detected and the multiple ligand loss in the formation of the lighter fragments observed, we expect the KER in the DEA processes to be even lower than that for the positive ion fragments.

Finally, the mass dependency of the transmission through the qudrupole mass spectrometer can cause significant discrimination against higher masses. To account for this effect for the positive ion formation, we have corrected the reported cross sections using the relative ion yields measured for N_2^+/N_2, Ar^+/Ar, Kr^+/Kr, and Xe^+/Xe, for which the absolute partial cross sections are well established.[34,39] The transmission data are extrapolated to m/z 145 and, as further extrapolation leads to negative values, the same correction factor is used for m/z 145 and 173. The transmission data are supplied as supplementary material.[40] The mass dependency of the transmission through the qudrupole mass spectrometer is probably the most significant error source, and for the positive ions we estimate the cross sections to be accurate within a factor of two. For the negative ions the transmission is optimized with respect to the SF_6^- signal and the mass difference between the calibrant; SF_5^-, and the main DEA fragments is much less than is the case for the positive ions. We have thus not corrected the DEA cross sections to account for mass discrimination, but we also estimate their accuracy to be generally within a factor of two. These might, however, be somewhat larger for the $[Co(CO)_2NO]^-$ formation close to 0 eV as well as the Co^- and $[CoCO]^-$ formation, especially at higher energies.

III. RESULTS AND DISCUSSION

A. Mass spectra

Positive fragment ions formed from $Co(CO)_3NO$ at 70 eV electron impact energy are summarized in Figure 1, in a stick mass spectrum, corrected for the mass dependent discrimination of the qudrupole mass spectrometer (see Sec. II B). The strongest signals in the mass spectrum are from the bare metal cation; Co^+, and the fragment $[CoCO]^+$, showing clearly that complete ligand loss is very efficient through DI at this energy. Albeit with a lower intensity, the parent cation is also discernible (m/z = 173). As observed previously by both electron impact and photodissociation studies,[38,41,42] metastable decay from the parent ion leads to the fragment $[Co(CO)_2NO]^+$ (m/z = 145) via loss of one carbonyl ligand while $[Co(CO)_3]^+$ formation is negligible. The subsequent loss of a second carbonyl group leads to $[CoCONO]^+$ (m/z = 117) while the loss of the nitrosyl group leads to $[Co(CO)_2]^+$ (m/z = 115). The fragment ion $[CoCO]^+$ (m/z = 87) can thus be formed through two different fragmentation pathways, i.e., the loss of a carbon monoxide ligand from $[Co(CO)_2]^+$ or the loss of a nitrogen monoxide ligand from $[CoCONO]^+$. The ion $[CoNO]^+$ (m/z = 89), on the other hand, is formed exclusively through the loss of a carbonyl ligand from $[CoCONO]^+$. This is likely to be the reason for the higher yield of $[CoCO]^+$ compared to $[CoNO]^+$. Finally, CoC^+ (m/z = 71) is observed as the only fragment where an internal ligand bond is broken rather than the metal-ligand bonds.

To our knowledge, there are two previous studies reporting positive ion formation from $Co(CO)_3NO$. Both of these report mass spectra recorded with sector field instruments at 50 and 70 eV incident energy, respectively. The relative intensities reported here agree well with these reported in the earlier study by Foffani *et al.*,[42] but not as well with those published more recently by Opitz.[41] This is particularly manifested through the relatively higher intensity of the larger fragments in the mass spectrum reported by Opitz.[41] A possible explanation for this is that for ions, which are formed with

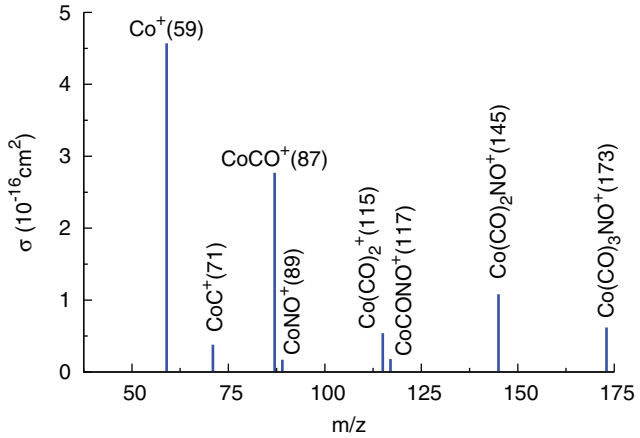

FIG. 1. Positive ion electron impact spectrum of $Co(CO)_3NO$ that results after collision with electrons of 70 eV incident electron energy. The cross sections were corrected for mass dependent discrimination in the extraction and the quadrupole mass spectrometer.

even low KER, a mass dependent discrimination will occur if the extraction aperture in to the mass spectrometer has a finite size. This effect, which is included in our corrections for the mass discrimination of the quadrupole mass spectrometer, favours heavier fragments, and depending on the extraction field and the geometry of the extraction region, this can potentially have a significant influence on the relative ratios observed in the respective mass spectra.

The extraction time in our spectrometer is around 10 μs while the flight time through the quadrupole mass filter is about 50 μs. However, as ions that fragment during the flight through the quadrupole filter do not maintain stable trajectories they will not be detected. Thus, the intensities reported here are snapshots of the fragment ions that are formed in the first 10 μs after the initial electron-molecule interaction, and are stable during their flight through the quadrupole mass filter. The same also applies for the negative ion formation.

Negative fragment ions formed in the energy range from about 0 to 9 eV are summarized in Figure 2, in a stick mass spectrum generated from the maximum cross section for each fragment. The dominant fragment formed through dissociative electron attachment to $Co(CO)_3NO$ is $[Co(CO)_2NO]^-$ (m/z = 145), which is formed by the loss of one carbonyl group. The ion $[Co(CO)_3]^-$ (m/z = 143), formed through the loss of the nitrogen oxide group, is about an order of magnitude less intense. This is readily understandable as the thermochemical threshold for NO loss is about 0.5 eV[21,41] higher than the threshold for CO loss, making the CO loss the only accessible DEA channel close to threshold (0 eV) where the electron attachment cross sections are very high (at low energies these cross sections generally increase as a function of $1/\varepsilon$, where ε is the incident electron energy). At sufficiently high internal energy, metastable decay and further loss of carbonyl ligands from $[Co(CO)_2NO]^-$ leads to the fragments $[CoCONO]^-$ (m/z = 117) and $[CoNO]^-$ (m/z = 89), while further loss of carbonyl ligands from $[Co(CO)_3]^-$ (m/z = 143) leads to $[Co(CO)_2]^-$ (m/z = 115) and $[CoCO]^-$ (m/z = 87). In addition, the loss of nitrogen oxide from $[Co(CO)_2NO]^-$ and $[CoCONO]^-$ can contribute to the intensities of the latter two fragments, which may explain why the $[CoCONO]^-$ and $[Co(CO)_2]^-$ intensities are comparable despite the higher threshold for $[Co(CO)_2]^-$ formation. The bare metal ion Co^- (m/z = 59) is also detected, but with low intensity and at a higher energy than the fragments ascribed to the sequential ligand loss described above. Its formation is attributed to a higher-lying core-excited (one-hole two-particle) resonance, that also leads to the formation of $[CoCO]^-$, but does not contribute to the ion yield of other fragments.[21] The parent anion is not observed in the negative ion mass spectra, which is presumably due to its lifetime, with regards to dissociation, being too short for it to be detected in our instrumental configuration.

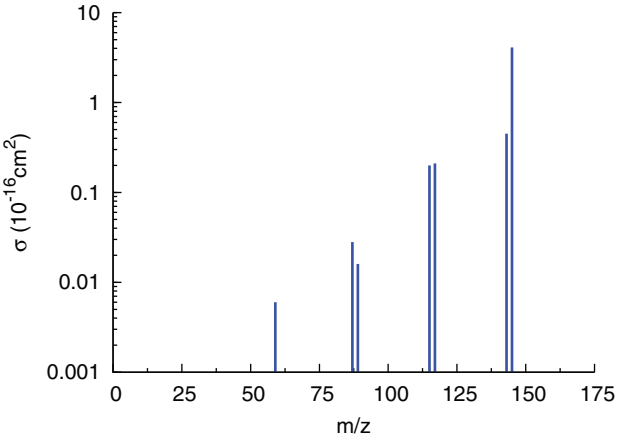

FIG. 2. Mass spectrum of the negative ion fragments formed at various incident electron energies. For each fragment, the maximum absolute cross section is depicted.

B. Cross sections

It is generally accepted that low energy SEs, i.e., electrons with energy <50 eV, play an important role in the deterioration of structures deposited by focused electron beams. We have recently presented absolute partial cross sections for fragment formation through DEA of cobalt tricarbonyl nitrosyl,[21] and relative cross sections for another standard FEBID precursor molecule trimethyl(methylcyclopentadienyl)platinum(IV).[22] These and other recent studies[23,24,43] reveal that DEA induces mainly incomplete fragmentation of the parent compound, in the energy range <10 eV, and may thus be responsible for the inclusion of non-metal contaminants in FEBID structures. However, as discussed earlier, dissociative ionisation is also operative in the secondary electron energy region, and for $Co(CO)_3NO$ this process leads predominantly to the formation of the bare metal cation, Co^+, through complete decomposition of the precursor. To be able to understand the importance of the DEA cross sections in relation to the DI cross sections, we here present absolute cross sections for all the dissociation pathways of these processes in the energy range from 0 to 140 eV. Table I thus compares the absolute cross sections for the fragments formed through electron impact at 70 eV with the maximum cross sections for the negative ions formed through DEA. The full energy range is depicted for the absolute partial cross sections in Figure 3 for DI and in Figure 4 for DEA, with the respective data files being supplied as supplementary material.[40]

TABLE I. Comparison between the positive and negative fragment ion absolute cross sections. The positive ion cross sections were measured at 70 eV, while the negative ion cross sections are reported at the energy of their maximum value.

Fragment	m/z	$\sigma(X^-)/10^{-16}$ cm^2	$\sigma(X^+)_{70eV}/10^{-16}$ cm^2
Co	59	<0.01	4.64
CoC	71	...	0.37
CoCO	87	0.03	2.77
CoNO	89	0.02	0.16
$Co(CO)_2$	115	0.2	0.53
CoCONO	117	0.2	0.17
$Co(CO)_3$	143	0.45	...
$Co(CO)_2NO$	145	4.1	1.13
$Co(CO)_3NO$	173	...	0.61

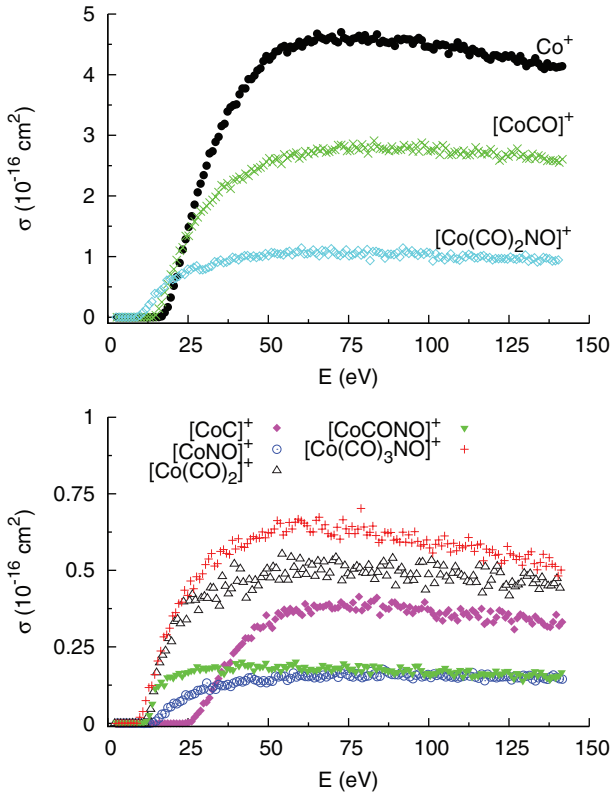

FIG. 3. Partial absolute cross sections for the cobalt containing positive fragment ions, as a function of the incident electron energy. See also the legend on the figures.

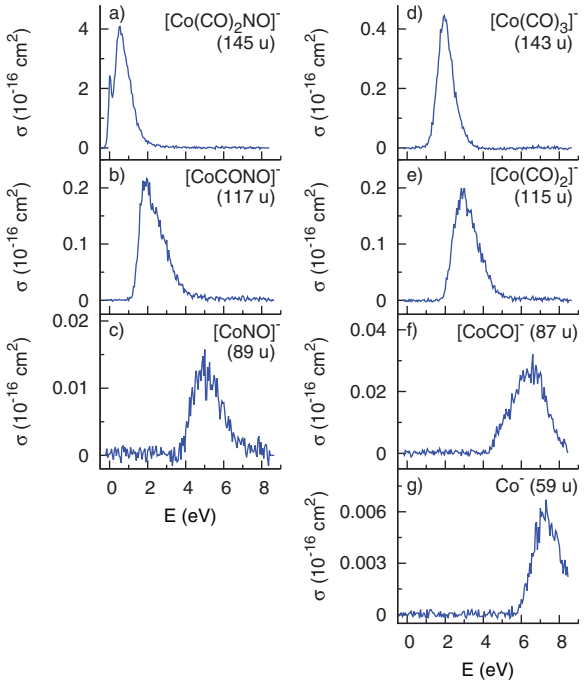

FIG. 4. Partial absolute DEA cross sections for $Co(CO)_3NO$, as a function of the incident electron energy (adapted from Ref. 21). See also the legend on the figures. Ion yields are background corrected.

Interestingly, the cross sections for negative ion formation through DEA and for positive ion formation through DI appear to be sort of inversed for the respective main fragments (see Table I). For instance, DEA results predominantly in the loss of one carbonyl group and thus forms $[Co(CO)_2NO]^-$ as the main fragment, with an estimated cross section of 4.1×10^{-16} cm^2. The corresponding DI cross section for $[Co(CO)_2NO]^+$ formation amounts to about 1.1×10^{-16} cm^2 (at 70 eV). The DI yield for Co^+ at 70 eV, on the other hand, surpasses 4.6×10^{-16} cm^2, while the formation of the bare Co^- anion is only a minor fragmentation pathway with a cross section of less than 0.01×10^{-16} cm^2. Furthermore, the second most intense fragment formed by DI is $[CoCO]^+$, with an approximate cross section of 2.8×10^{-16} cm^2 (at 70 eV), while the corresponding DEA cross section for the $[CoCO]^-$ formation is only about 0.03×10^{-16} cm^2. Similarly, the second most intense fragment formed by DEA; $[Co(CO)_3]^-$, is formed with a cross section of about 0.45×10^{-16} cm^2, while the corresponding DI fragment; $[Co(CO)_3]^+$, is not detectable. A further noteworthy difference between DI and DEA is the DI fragment CoC^+. This is the only fragment we detect where ligand fragmentation is observed, albeit with a relatively high threshold of slightly above 22 eV, the cross section at 70 eV is about 0.37×10^{-16} cm^2.

It is clear from both Figures 3 and 4 that the partial cross sections for the individual channels depend strongly on the incident electron energy. This is particularly visible for the DEA cross sections, but also holds true for the DI processes close to threshold. While at 0 eV, $[Co(CO)_2NO]^-$ is formed almost exclusively, the cross section for the formation of this fragment is already close to zero at about 2 eV incident electron energy, and by 7 eV the only DEA fragments detected are $[CoCO]^-$ and Co^-. At slightly higher energies, DEA is no longer active and DI becomes energetically accessible and dominates the total cross section. The appearance potentials (APs) for the individual DI processes range from about 9–15 eV for the ligand losses, and the AP is close to 22 eV for the formation of CoC^+.[38,41] Thus, in this energy range, the partial DI cross sections are strongly dependent on the incident electron energy. In FEBID, the energy distribution of the PEs, SEs, and BSEs is thus going to determine the relevance of these fragmentation channels in the deposition process. The upper panel in Figure 5, therefore, compares the total cross section for ion formation from $Co(CO)_3NO$ through DEA and DI, as a function of incident electron energy, in the energy range from 0–140 eV. The cross section data are plotted on a logarithmic scale for better visibility, and are superimposed with a calculated and experimental SE spectrum for nickel (111) irradiated with 400 eV electrons.[20] The maximum SE yield lies at around 3 eV, so there is a considerable overlap of the SE energy distribution with the energy region where DEA is the most efficient fragmentation channel. The tail of the SE energy distribution, on the other hand, overlaps with the DI onset, where DEA is no longer operative. In the lower panel of Figure 5, the relative effective damage yield, derived from the product of the total ion yields and the normalized, measured SE yield, is shown for the same energy range. It is clear from Figure 5 that, though the DEA cross sections are confined to a rather narrow energy window, the maximum

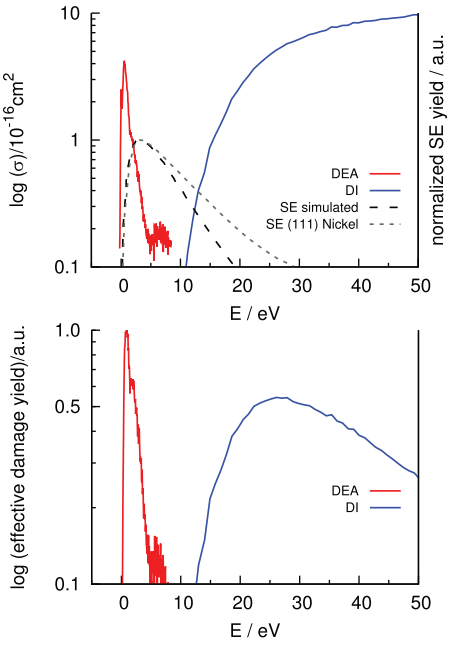

FIG. 5. In the upper panel, the combined total cross sections for DEA and DI of $Co(CO)_3NO$ is shown for E < 50 eV. Also shown are the normalized secondary electron (SE) yields, both calculated and measured. See legend in the figure for further details. In the lower panel, the normalized effective damage yield for DEA and DI of $Co(CO)_3NO$ is shown in the same energy range. The effective damage yield is derived from the product of the total ion yields and the normalized experimental SE yield.

effective damage yield for DEA is about twice that for DI. However, it is also clear from this figure that the integral effective damage yield for DI (up to 50 eV) is about six fold compared to DEA. Hence, considering the high SE yield, it is clear that both these processes are likely to play a significant role in FEBID.

It should, however, be kept in mind that, especially the DEA channels, may be very sensitive to the surrounding medium. Thus, enhancement, but also quenching of particular DEA channels, may occur when the precursor molecules are adsorbed on surfaces.[44] Nonetheless, using gas phase cross sections is a valid approach, in order to elucidate the different processes occurring at the surface (for a review on the subject, see Ref. 45), and DI cross sections have been successfully adapted for use in MC simulations (e.g., see Refs. 29 and 27). To our knowledge, however, DEA has to date not been accounted for in MC simulations dealing with FEBID, and although it is clear that further studies are necessary to confirm their relevance and especially how the DEA processes are influenced by the supporting surface, recent investigations indicate strongly that DEA may play a pivotal role in FEBID.[21–25,46] In particular, this applies to the purity of the deposit and the broadening of the deposits beyond the diameter of the electron beam, which are currently the main challenges that need to be addressed to further enhance the applicability of FEBID as a standard tool in nano-fabrication. Like DEA, absolute cross sections for DI of relevant FEBID precursor molecules are scarce. We thus believe that the currently presented absolute DEA and DI cross sections provide valuable information in order for us to try and understand the processes governing FEBID at the nanoscale.

IV. CONCLUSIONS

In this contribution, we have presented a detailed set of cross sections for both DEA and DI of the FEBID precursor cobalt tricarbonyl nitrosyl. A comparison of the cross sections for the different fragmentation mechanisms resulted in several implications relevant to FEBID: DEA is highly efficient in an energy region where the intensity of the SEs has its maximum, i.e., below 10 eV. The most intense DEA channel is the cleavage of one Co–CO bond, while further fragmentation is less significant and the formation of the bare Co^- metal anion is insignificant. DEA can thus be expected to contribute mainly to the deposition of incompletely dissociated precursor molecules, which in turn increases the fraction of nonmetallic contaminants in the deposit. Dissociative ionization, while energetically accessible only through the tail of the SE energy distribution, is a very efficient process for Co^+ formation. Thus, DI induced through SEs is more likely to contribute to Co deposition and less to the deposition of incompletely dissociated precursor molecules, and as the primary electron beam induces a considerable flux of SEs outside the focal point of the beam, this is likely to contribute significantly to the broadening of the deposit. Nevertheless, these are qualitative conclusions, based on the overlap of the SE yield with the energy range relevant for the respective DEA and DI processes, so it would be desirable to include the reported cross sections in MC simulations of the deposition to try to establish a more quantitative picture of their role in FEBID.

ACKNOWLEDGMENTS

This work was supported by the Icelandic Centre for Research (RANNIS), Slovak Research and Development Agency (Project Nos. APVV-0733-11 and DO7RP-0025-11), project named VEGA 1/0514/12, and is also the result of the project implementation: 26240120012 and 26240120026 supported by the Research & Development Operational Programme funded by the ERDF. S.E. gratefully acknowledges funding for the visit to Bratislava from the ECCL COST Action CM0601 and a Ph.D. grant from Rannsóknasjóður Háskóla Íslands. One of us (M.J.B.) also acknowledges funding from the Australian Research Council through their Centre of Excellence program. The authors like to thank Benedikt Ómarsson for his help with the ion trajectory simulations.

[1] S. Gambarotta and H. Alper, J. Organomet. Chem. **212**, C23 (1981).
[2] D. Dhar, Y. Koltypin, A. Gedanken, and S. Chandrasekaran, Catal. Lett. **86**, 197 (2003).
[3] A. R. Ivanova, G. Nuesca, X. Chen, C. Goldberg, A. E. Kaloyeros, B. Arkles, and J. J. Sullivan, J. Electrochem. Soc. **146**, 2139 (1999).
[4] N. Papadopoulos, C. S. Karayianni, P. Tsakiridis, E. Sarantopoulou, and E. Hristoforou, Chem. Vap. Deposition **17**, 211 (2011).
[5] A. R. Londergan, G. Nuesca, C. Goldberg, G. Peterson, A. E. Kaloyeros, B. Arkles, and J. J. Sullivan, J. Electrochem. Soc. **148**, C21 (2001).
[6] H. S. Rhee and B. T. Ahn, J. Electrochem. Soc. **146**, 2720 (1999).
[7] I. Utke, P. Hoffmann, and J. Melngailis, J. Vac. Sci. Technol. B **26**, 1197 (2008).
[8] W. F. van Dorp and C. W. Hagen, J. Appl. Phys. **104**, 081301 (2008).
[9] M. H. Ervin and B. M. Nichols, J. Vac. Sci. Technol. B **27**, 2982 (2009).
[10] Y. M. Lau, P. C. Chee, J. T. L. Thong, and V. Ng, J. Vac. Sci. Technol. A **20**, 1295 (2002).
[11] I. Utke, P. Hoffmann, R. Berger, and L. Scandella, Appl. Phys. Lett. **80**, 4792 (2002).

[12]M. Gabureac, L. Bernau, I. Utke, and G. Boero, Nanotechnology **21**, 115503 (2010).
[13]G. C. Gazzadi, H. Mulders, P. Trompenaars, A. Ghirri, M. Affronte, V. Grillo, and S. Frabboni, J. Phys. Chem. C **115**, 19606 (2011).
[14]A. Fernández-Pacheco, J. M. De Teresa, R. Cordoba, and M. R. Ibarra, J. Phys. D **42**, 055005 (2009).
[15]R. Solanki, P. K. Boyer, J. E. Mahan, and G. J. Collins, Appl. Phys. Lett. **38**, 572 (1981).
[16]G. C. Gazzadi, J. J. L. Mulders, P. Trompenaars, A. Ghirri, A. Rota, M. Affronte, and S. Frabboni, Microelectron. Eng. **88**, 1955 (2011).
[17]I. Utke, J. Michler, P. Gasser, C. Santschi, D. Laub, M. Cantoni, P. A. Buffat, C. Jiao, and P. Hoffmann, Adv. Eng. Mater. **7**, 323 (2005).
[18]A. Botman, M. Hesselberth, and J. J. L. Mulders, Microelectron. Eng. **85**, 1139 (2008).
[19]A. Botman, J. J. L. Mulders, and C. W. Hagen, Nanotechnology **20**, 372001 (2009).
[20]J. Schaefer and J. Hoelzl, Thin Solid Films **13**, 81 (1972).
[21]S. Engmann, M. Stano, Š. Matejčík, and O. Ingólfsson, Angew. Chem., Int. Ed. **50**, 9475 (2011).
[22]S. Engmann, M. Stano, Š. Matejčík, and O. Ingólfsson, Phys. Chem. Chem. Phys. **14**, 14611 (2012).
[23]M. Allan, J. Chem. Phys. **134**, 204309 (2011).
[24]O. May, D. Kubala, and M. Allan, Phys. Chem. Chem. Phys. **14**, 2979 (2012).
[25]K. Landheer, S. G. Rosenberg, L. Bernau, P. Swiderek, I. Utke, C. W. Hagen, and D. H. Fairbrother, J. Phys. Chem. C **115**, 17452 (2011).
[26]N. Silvis-Cividjian, C. W. Hagen, L. H. A. Leunissen, and P. Kruit, Microelectron. Eng. **61–62**, 693 (2002).
[27]J. D. Fowlkes, S. J. Randolph, and P. D. Rack, J. Vac. Sci. Technol. B **23**, 2825 (2005).
[28]D. A. Smith, J. D. Fowlkes, and P. D. Rack, Nanotechnology **18**, 265308 (2007).
[29]N. Silvis-Cividjian, C. W. Hagen, and P. Kruit, J. Appl. Phys. **98**, 084905 (2005).
[30]C. W. Hagen, W. F. van Dorp, P. A. Crozier, and P. Kruit, Surf. Sci. **602**, 3212 (2008).
[31]M. Stano, Š. Matejčík, J. D. Skalny, and T. D. Märk, J. Phys. B **36**, 261 (2003).
[32]A. Stamatovic and G. J. Schulz, Rev. Sci. Instrum. **39**, 1752 (1968).
[33]S. G. Lias, "Ion Energetics Data," in *NIST Chemistry WebBook, NIST Standard Reference Database Number 69*, Eds. P. J. Linstrom and W. G. Mallard, National Institute of Standards and Technology, Gaithersburg MD, 20899, http://webbook.nist.gov (retrieved October 05, 2013).
[34]R. Rejoub, B. G. Lindsay, and R. F. Stebbings, Phys. Rev. A **65**, 042713 (2002).
[35]M. Braun, S. Marienfeld, M. W. Ruf, and H. Hotop, J. Phys. B **42**, 125202 (2009).
[36]M. Fenzlaff, R. Gerhard, and E. Illenberger, J. Chem. Phys. **88**, 149 (1988).
[37]M. Fieber-Erdmann, E. Holub-Krappe, G. Bröker, G. Dujardin, and A. Ding, Int. J. Mass Spectrom. Ion Process. **149/150**, 513 (1995).
[38]B. Sztaray and T. Baer, J. Phys. Chem. A **106**, 8046 (2002).
[39]H. C. Straub, P. Renault, B. G. Lindsay, K. A. Smith, and R. F. Stebbings, J. Phys. Rev. A **54**, 2146 (1996).
[40]See supplementary material at http://dx.doi.org/10.1063/1.4776756 for data files of the positive and negative ion cross sections as a function of incident electron energy.
[41]J. Opitz, Int. J. Mass Spectrom. **225**, 115 (2003).
[42]A. Foffani, S. Pignataro, G. Distefano, and G. Innorta, J. Organomet. Chem. **7**, 473 (1967).
[43]K. Wnorowski, M. Stano, C. Matias, S. Denifl, W. Barszczewska, and Š. Matejcík, Rapid Commun. Mass Spectrom. **26**, 2093 (2012).
[44]I. Bald, J. Langer, P. Tegeder, and O. Ingólfsson, Int. J. Mass Spectrom. **277**, 4 (2008).
[45]C. D. Lane and T. M. Orlando, Appl. Surf. Sci. **253**, 6646 (2007).
[46]J. D. Wnuk, J. M. Gorham, S. G. Rosenberg, W. F. van Dorp, T. E. Madey, C. W. Hagen, and D. H. Fairbrother, J. Phys. Chem. C **113**, 2487 (2009).